### Title

Observations of bedload transport in a gravel bed river during high flow using fiber-optic DTS methods




### Journal

Earth Surface Processes and Landforms, 42(13)

### ISSN

0197-9337



### Authors

Bray, Erin N
Dunne, Thomas



### Publication Date

2017-10-01

### DOI

10.1002/esp.4164

Peer reviewed

EARTH SURFACE PROCESSES AND LANDFORMS
*Earth Surf. Process. Landforms* (2017)

Published online in Wiley Online Library
(wileyonlinelibrary.com) DOI: 10.1002/esp.4164

# Observations of bedload transport in a gravel bed river during high flow using fiber-optic DTS methods

**Erin N. Bray[1,2]* and Thomas Dunne[3]**
[1] Earth Research Institute, University of California, Santa Barbara, CA USA
[2] Center for Environmental Design Research, University of California, Berkeley, CA USA
[3] Bren School of Environmental Science and Management, University of California, Santa Barbara, CA USA

Received 30 April 2016; Revised 22 March 2017; Accepted 18 April 2017

*Correspondence to: Erin Bray, Earth Research Institute, University of California, Santa Barbara, CA 93106, USA. E-mail: ebray@bren.ucsb.edu

ESPL
Earth Surface Processes and Landforms

ABSTRACT: The question: 'how does a streambed change over a minor flood?' does not have a clear answer due to lack of measurement methods during high flows. We investigate bedload transport and disentrainment during a 1.5-year flood by linking field measurements using fiber optic distributed temperature sensing (DTS) cable with sediment transport theory and an existing explicit analytical solution to predict depth of sediment deposition from amplitude and phase changes of the diurnal near-bed pore-water temperature. The method facilitates the study of gravel transport by using near-bed temperature time series to estimate rates of sediment deposition continuously over the duration of a high flow event coinciding with bar formation. The observations indicate that all gravel and cobble particles present were transported along the riffle at a relatively low Shields Number for the median particle size, and were re-deposited on the lee side of the bar at rates that varied over time during a constant flow. Approximately 1–6% of the bed was predicted to be mobile during the 1.5-year flood, indicating that large inactive regions of the bed, particularly between riffles, persist between years despite field observations of narrow zones of local transport and bar growth on the order ~3–5 times the median particle size. In contrast, during a seven-year flood approximately 8–55% of the bed was predicted to become mobile, indicating that the continuous along-stream mobility required to mobilize coarse gravel through long pools and downstream to the next riffle is infrequent. Copyright © 2017 John Wiley & Sons, Ltd.

KEYWORDS: sediment transport; river; gravel; bedload; fiber optic DTS

## Introduction

Little is known about the entrainment, transport, and disentrainment of coarse sediment during floods in gravel bed rivers due to lack of measurement methods during high flows. While a number of studies define conditions for incipient motion (Lamb *et al*., 2008), few studies address the occurrence, patterns, and rates of disentrainment of gravel bed material. Thus, it is not always possible to recognize how physical processes that scour, transport, and deposit grains control bedform evolution, to distinguish between active and inactive zones of transport, or to predict how flow pulses affect the depositional processes by which the complex form and sedimentological architecture of gravel bed rivers develop.

In some rivers, a substantial portion of the bed material transported over a period of years is carried under marginal or partial transport, a condition when relatively few bed particles are moving at any time (Andrews, 1994). During this condition, many grains or zones remain inactive, and even active grains or zones typically spend most of the time immobile (Wilcock and McArdell, 1997; Haschenburger and Wilcock, 2003). As a result, collecting direct field measurements of the portion of the bed that becomes active – at the onset of motion – presents a challenge to monitoring the limited but persistent occurrence of transport during intermediate-sized floods that shape channels and their bedforms and also maintain spawning habitat for fish species (Geist and Dauble, 1998). Key uncertainties also persist in understanding the nature, extent, magnitude, timing and rate of bedload movement, disentrainment and bed elevation changes during these flows and their relationships to calculated transport conditions.

Owing to the difficulty of measuring bedload transport during high flows, and the general skepticism of the relative merits of sediment transport formulae applied to rivers unlike those in which they were calibrated, various methods have been used to establish field-based fluxes for bedload transport. The traditional approach has been to measure bedload transport rates using a handheld Helley–Smith sampler at several locations over the course of several days, or by using trough or pit samplers into which bedload particles drop (Hubbell, 1964; Leopold and Emmett, 1976; Church and Hassan, 2002). Because large temporal and spatial variability are often observed in bedload transport rates, it is difficult to collect a sufficient number of samples over long periods of time or continuously along a reach. Scour, fill, and burial depths

have been measured using magnetically-tagged particles and/or scour chains (Emmett and Leopold, 1963; Hassan, 1990; Laronne *et al.*, 1994), while changes in bed elevation at larger spatial scales have been measured using remote sensing for geomorphic change detection (Wheaton *et al.*, 2010). More recently, transport rates have been measured using a wide variety of passive sensors including geophones in contact with the streambed, hydrophones deployed in the water column, impact columns, and magnetic detection (Gray *et al.*, 2010). The most developed of these approaches involves the installation and calibration of acoustic geophones mounted under steel plates or pipes in the streambed which record the vibrations of particles moving across the plates (Rickenmann and McArdell, 2007). Other passive methods used to record the timing of scour and fill have utilized accelerometer scour monitors (Gendaszek *et al.*, 2013) and time domain reflectometry (TDR) which can detect transport of sediment sizes of less than 1 cm (Chung and Lin, 2011; Chung *et al.*, 2013; Miyata and Fujita, in review). While these methods have enabled measurement of the start and end of transport, scour, and fill events, a limitation of both passive and active methods is that they cover a surface area on the order of tens of centimeters, often require some disturbance of the bed during installation, and require different methods for sand and gravel. With the exception of TDR, most methods are unable to detect transport of sediment sizes of less than 1 cm diameter (Turowski *et al.*, 2011) or detect bed elevation changes that are within the resolution of the digital elevation detection error (Milan *et al.*, 2011).

As such, several distinctive features of bedload transport in gravel bed rivers are not adequately recorded through existing measurement methods. First, their tendency to scour and deposit sediment in narrow active zones, which in turn adjust to changes in discharge and sediment supply, result in episodic, partial or full transport events that occur in otherwise relatively stable beds. Second, their propensity to generate and maintain bedforms in a pattern of alternating bar and pool morphology make them susceptible to exacerbating sediment-deficit or sediment-excess conditions with adjustments to the flow and sediment supply, which in turn affects the along-stream variations in channel bed composition. Third, little is known about the spatial and temporal continuity of transport between riffle and pool and therefore the conditions required to maintain both features.

We present a field and modeling investigation of the onset, endpoint, and rate of change of bedload transport and disentrainment during a regulated, constant flow with a recurrence interval of 1.5 years in a lowland gravel-bed river. We installed 2 km of fiber-optic distributed temperature sensing (DTS) cable directly on top of the riverbed over the length of three pool-riffle sequences during an ongoing large-scale flow experiment that was designed for the re-introduction of salmon. We took advantage of the fact that some portions of the DTS cable that we had deployed became inundated with sediment during the flow release, and the extent, time, and rate of that inundation could be calculated by inverting changes in the amplitude and phase of the water temperature signal with the use of a theory originally developed for a sand bed stream (Luce *et al.*, 2013; Tonina *et al.*, 2014). Fiber-optic DTS systems have been widely used for industrial applications and have recently been employed to detect groundwater exchange in fluvial environments (Selker *et al.*, 2006; Tyler *et al.*, 2009), but to our knowledge ours is the first application used to detect sediment transport.

We use the results from the field investigation to identify the occurrence, timing, and locations of bedload deposition, and therefore of transport and entrainment, which were verified by measuring the thickness of the deposition overlying the cable at the end of the flow event and which allowed us to calculate directly the thermal properties of that sediment. We then utilize the measured patterns of disentrainment to validate our attempt to calculate bed mobility with several bedload transport formulae and to illustrate the reach-scale spatial patterns of our observations. We then implemented the bedload transport formulae for a larger hypothetical flood to examine how riffle-pool sequences in this sediment starved lowland gravel-bed river maintain their form during floods of moderate size and frequency. In particular, we address the following questions:

1. Can high-resolution spatiotemporal measurements of near-bed water temperature be used to understand the nature of streambed changes during a flood?
   a. Is there evidence of mobility, scour, or fill?
   b. What is the total accumulation of gravel?
   c. What is the rate of disentrainment of gravel?
2. How do the riffle-pool sequences in this sediment-starved lowland gravel bed river maintain their form?

Our analysis shows that disentrainment and deposition processes can be extracted solely from the time series of pore-water temperatures recorded by the fiber-optic DTS cable during its burial by the accumulating sediment, once the depth of sediment is measured at the beginning and end of the experiment to allow the thermal properties of the sediment to be calculated (Figure 1). The results demonstrate that the discharge needed to entrain all particle sizes in gravel-cobble riffle reaches is lower than standard expectations and the rates of sediment disentrainment over space and time are not constant during a constant-intensity minor flood pulse.

The method establishes a new direction of inquiry on bedload transport during floods coinciding with gravel bar formation and modification, and introduces a new method by which bedload transport of gravel and sand might be measured *in situ* continuously during high flows at a high spatial and temporal resolution.

## Theoretical Discussion

Deposition and scour in riverbeds can change the amplitude and phase of temperature time series collected at two fixed elevations in the bed. For sensors located at depths 1 and 2, the temperature amplitude ratio, $A_r$, and phase shift, $\Delta\phi$, were defined by Stallman (1965) as:

$$A_r = \frac{A_2}{A_1} \tag{1}$$

$$\Delta\phi = \phi_2 - \phi_1 \tag{2}$$

where $A$ is the amplitude, $\phi$ is the phase, and subscripts 1 and 2 denote two different depths in the streambed. Stallman (1965) showed that the phase lag of a sinusoidal temperature signal increases and the amplitude is dampened with increasing streambed depth. Following Luce *et al.* (2013) and Tonina *et al.* (2014), the amplitude and phase of the

temperature of the water in porous media can be expressed as the dimensionless fluid velocity

$$\eta = \frac{-\log\left(\frac{A_2}{A_1}\right)}{\phi_2 - \phi_1} = \frac{-\log(A_r)}{\Delta\phi}. \tag{3}$$

The ratio of the log-amplitude ratio to the phase difference, $\eta$, is simply a function of measured quantities from which the effective thermal diffusivity of the streambed sediment, $K_e$, can be quantified from measurements of temperature. The solution of $K_e$ is given by

$$K_e = \frac{\omega \Delta z^2}{\Delta\phi^2} \frac{\eta}{1+\eta^2} \tag{4}$$

where $\omega = 2\pi/P$, $P$ is the period of the temperature signal (one day), and $\Delta z$ is the difference of the sediment thickness between the two sensor locations.

Tonina *et al.* (2014) showed that if the total sediment thickness, $\Delta z$, is measured directly at any given timestep, and thus the thermal diffusivity is known from Equations (3) and (4), then temporal variations in the bed elevation can be calculated by:

$$\Delta z = \Delta\phi \sqrt{\frac{K_e}{\omega}\left(\eta + \frac{1}{\eta}\right)} \tag{5}$$

If the diffusivity is known, uniform, and constant over the daily timescale, variations in the thickness of the sediment can be calculated via Equation (5). A key aspect of using this approach to quantify sedimentation processes in gravel bed rivers lies in the ability to compute $K_e$ directly from field measurements. As formulated, Equation (4) should apply to any mixture of gravel and sand, from uniform to poorly sorted, so long as the depth of sediment at a given timestep is known and the composition of the sediment is relatively constant at a single location over the time period for which all other values of $\Delta z$ are calculated.

The solution for $\Delta z$ in Equation (5) was originally formulated to assess a vertical pair of temperature probes: one located at the streambed surface and one at some depth into the bed (Luce *et al.*, 2013). In this study, we instead apply the Luce *et al.* (2013) formulation to the case of a fiber-optic DTS cable that continuously records near-bed temperature at regular intervals over time and along its length. Thus, $\Delta z$ can be found by pairing two or more discrete locations (horizontal) over distance – one which constantly measures near-bed temperature at a streambed surface location without deposition, and another nearby streambed surface location whose temperature is modified by sediment transport and

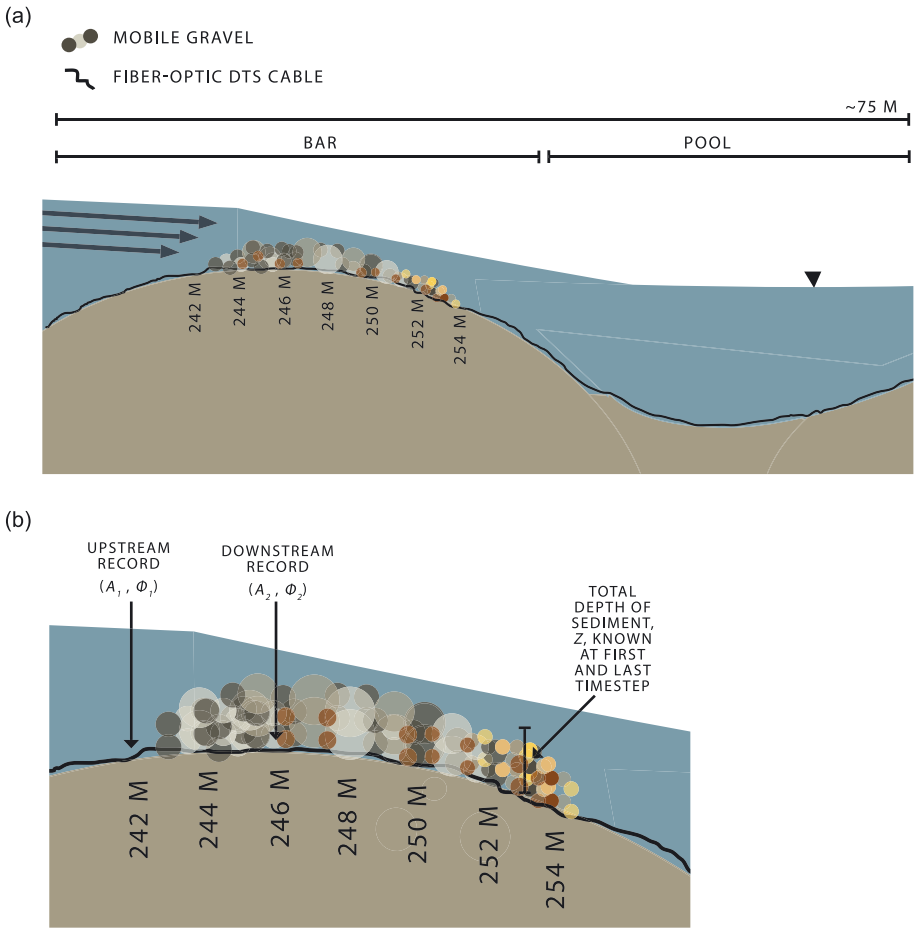


**Figure 1.** Schematic diagram of sediment disentrainment evaluated over the length of a gravel bed reach coinciding with a 10-day, constant-intensity, sediment-mobilizing flow event. Schematic diagram in (a) shows the field installation of fiber-optic distributed temperature sensing (DTS) cable, which recorded temperature at approximately 2-m intervals along a cable positioned at the riverbed over the length of a 2-km gravel bed reach of the San Joaquin River, CA, USA. (b) Schematic diagram of the measurements used to calculate $\Delta z$. [Colour figure can be viewed at wileyonlinelibrary.com]

deposition and thus by changes in the overlying sediment thickness over time. As such, subscripts 1 and 2 in Equations (1) and (2) here denote two different temperature locations along the length of a fiber-optic DTS cable (Figure 1b). A bed-surface temperature record at a stable location is paired with the temperature record from a sensor that is initially at the bed surface, but which becomes buried to a known depth at the end of the time series. Here we assume that – for the period that deposition is tracked – $K_e$ is constant over time, depth invariant, can be estimated from a time period when $\Delta z$ is known, but can vary spatially owing to different locations in which gravel and sand tend to be deposited on the bed. This interpretation is based on the observation that sediment thermal properties are commonly time invariant. While Rau *et al.* (2015) showed that the thermal diffusivity calculated using field data (e.g. Tonina *et al.* [2014]) can exceed physically possible values during highly transient flow conditions, they concluded that the quantification of time-variable sediment scour/deposition from temperature records in combination with diurnally forced analytical solutions are reliable when discharge is not highly transient.

In the current context, the analysis applies to sediment deposition only (not scour), but could be adapted to calculate both scour and deposition with the installation of a second sensor at a second depth. We neglect compaction of the sediments in the bed and changes in subsurface flow because the sediment is coarse, the discharge is constant, and because compaction is likely to be negligible over the duration of our observations. We assume that the diurnal cycle of ambient stream water temperature (due to atmosphere–water interactions) is relatively constant over the distance of our domain. We pay detailed attention to the changes in bed elevation coinciding with gravel bar evolution during a 10-day constant, managed flow event because the thermal properties can be calculated directly from field measurements, because the flow remained steady, and because of its relevance to habitat and management.

## Methods

### Study area

This study took place along a 2-km reach of the San Joaquin River 13.3 to 15.3 km (river miles 259.7 and 258.5) downstream of Friant Dam near Fresno, California, USA (Figure 2a) where the drainage area is ~4,340 km$^2$. The San Joaquin River originates in the Sierra Nevada range and flowing west-southwest through the Central Valley before turning north to the confluence of the Sacramento River and the San Francisco Bay Delta. The flow regime at Friant Dam is controlled primarily by reservoir regulation, irrigation storage, and a combination of rainstorm events in late fall and winter and snowmelt runoff in late spring. For two years prior to our study, the San Joaquin River downstream of Friant Dam has been the subject of an ongoing large-scale flow experiment during which interim flow releases were designed for the purposes of restoring salmon habitat (Figure 3a).

The study reach (Figure 2b) is a gravel-bedded channel with low-sinuosity bends expressed as riffle-pool sequences along a mainstem branch of a split-flow channel around a large fluvial island ('Rank Island'). The gravel bed reach of the San Joaquin River has a mean bankfull width of approximately 60 m and mean bankfull depth of 0.85 m with a water-surface gradient of 0.00059. The riffles average 150 m in length and alternate with pools and runs that average 1200–1500 m in length. In the 2-km study area, each of the riffle-pool sequences consists of a deep pool upstream of a low-amplitude bend that widens and shoals to an oblique riffle crest and lateral bar. Opposite the bar is a narrow, deep scour hole (pool) coinciding with the apex of the bend that shoals to a second elongated point or mid-channel bar. The riffles are referred to locally as riffle clusters because they consist of widely separated couplets of a point bar followed by a second elongated mid-channel or point bar. The bars are the eroded remnants of larger bars within the channel that had been maintained by the pre-dam flow regime and gravel supply. The current study is focused on the two riffles identified in Figure 2b as Riffle 1 and Riffle 2.

Median grain size of the bed material varies from a minimum of approximately 10 mm in deep sand-bedded pools/runs to a maximum of approximately 60–120 mm in gravel riffles (Figure 3b). Field surveys using the Wolman pebble count method and bulk samples (California Department of Water Resources, 2010; US Bureau of Reclamation, 2014a) in Riffle 1 indicate that the surface is composed of cobbles and coarse gravel, with a median particle size of 64 mm ($D_{84}$ = 80 mm). In Riffle 2, the surface has a median particle size of 82 mm ($D_{84}$ = 114 mm). The percent gravel ranges from ~70 to 95% throughout the 2-km study reach, while the remaining fraction is comprised mostly of sand.

Discharge along the reach is measured continuously at US Geological Survey (USGS) gage 11251000 located approximately 9 km upstream of our study site. A log-Pearson Type III flood frequency analysis of the pre-dam dam flow regime (1908–1942) indicates that the two-year flood (Q2) corresponded to a discharge of 388 m$^3$ s$^{-1}$ and the 10-year flood (Q10) to a discharge of approximately 1017 m$^3$ s$^{-1}$. In the post-dam flow regime (1943–2012) the Q2 has decreased to 44 m$^3$ s$^{-1}$ and the Q10 to 321 m$^3$ s$^{-1}$.

The field investigation was conducted during three sequential steady discharge events within a continuous 32-day sequence (1.5 days at 10 m$^3$ s$^{-1}$, 10 days at 20 m$^3$ s$^{-1}$, 16 days at 10 m$^3$ s$^{-1}$, and 4.5 days at 2–4 m$^3$ s$^{-1}$) during the period October 10, 2011–November 10, 2011. We pay detailed attention to the 10-day pulse flow of 20 m$^3$ s$^{-1}$, which is roughly half of a bankfull flow and corresponds to the post-dam 1.5-year flood (Q1.5) (US Bureau of Reclamation, 2013).

### Field investigation

We deployed 2 km of fiber-optic DTS cable directly on top of the riverbed over three pool-riffle sequences. The cable consisted of two separate segments, each containing two co-located fibers and each connected to the DTS unit, beginning with 700 m at the upstream extent followed by 1300 m immediately downstream. During the installation, a combination of concrete pavers and zip ties, weights, cobbles or stakes were used to secure the cable in place periodically along the reach. The position of the cable is shown by the blue line in Figure 2b. The cable was installed along the thalweg except at each location of a deep scour hole at the apex of a bend. At those locations the current was too strong even at wadeable flows during the installation (10 m$^3$ s$^{-1}$), so we instead installed the cable up along the inundated portion of the opposite bar and inward of the thalweg.

Fiber-optic DTS along multimode fiber-optic cable was employed using a Sensornet Halo DTS system (Sensornet Ltd, Borehamwood, UK) and armored Kaiphone fiber-optic cable (Kaiphone Technology Co. Ltd, Dongguan, China). Fiber-optic DTS technology uses Raman spectra scattering in an optical fiber to measure temperature along its length, i.e. the fiber-optic

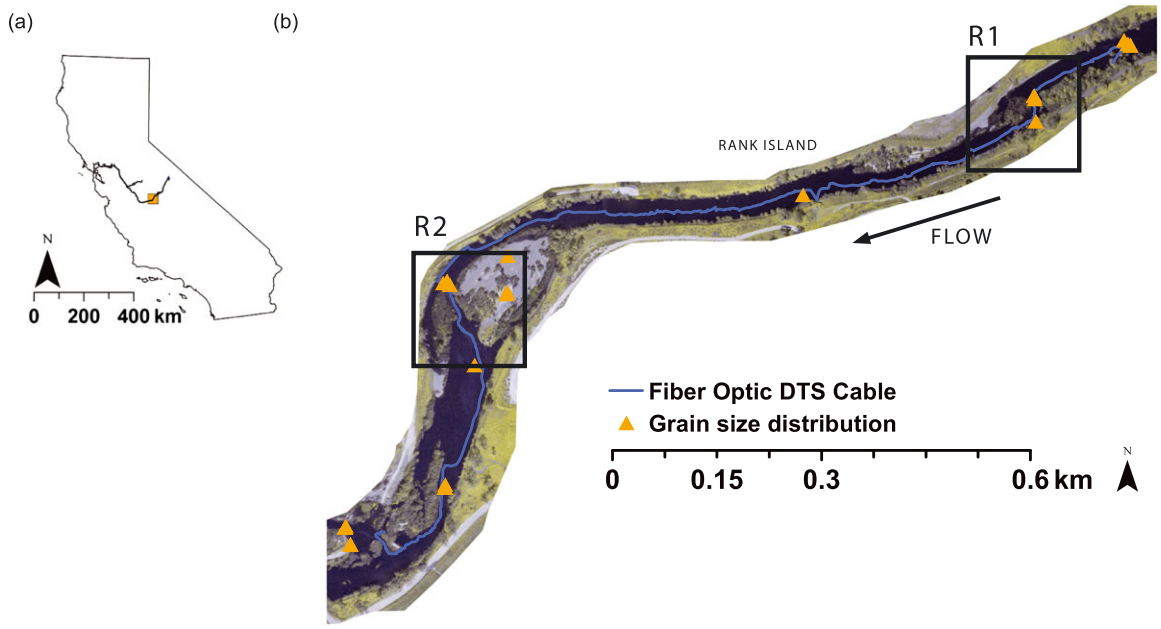


**Figure 2.** (a) Location of the 2-km study area located approximately 13 km downstream of Friant Dam on the San Joaquin River near Fresno, CA, USA. (b) Detailed aerial map of the 2-km study reach and locations of each of two riffle-pool reaches upon which this study is focused, referred to as Riffle 1 (upstream, R1) and Riffle 2 (downstream, R2). Also indicated is the position of the fiber optic distributed temperature sensing (DTS) cable and the locations at which point measurements of grain size distributions were previously taken. [Colour figure can be viewed at wileyonlinelibrary.com]

cable is the thermometer (Selker *et al.*, 2006). We employed a duplexed, single-ended installation involving two co-located fibers within one cable following the same path and spliced together at the end. This allows two temperature observations to be recorded at every point along the cable with a single connection to the DTS instrument. The instrument then makes observations from both directions on a looped and spliced cable that has both ends connected to the DTS system. Duplexed observations allow for the correction for non-uniform attenuation of light along the entire length of the cable. For details regarding the principles of Raman scattering and spatial resolution underlying DTS applications, the reader is referred to Suárez *et al.* (2011).

Reference sections illustrated in Figure 4 were configured in the field using 20-m sections of cable at known and uniform temperature. Reference sections consisted of: (1) a warm bath

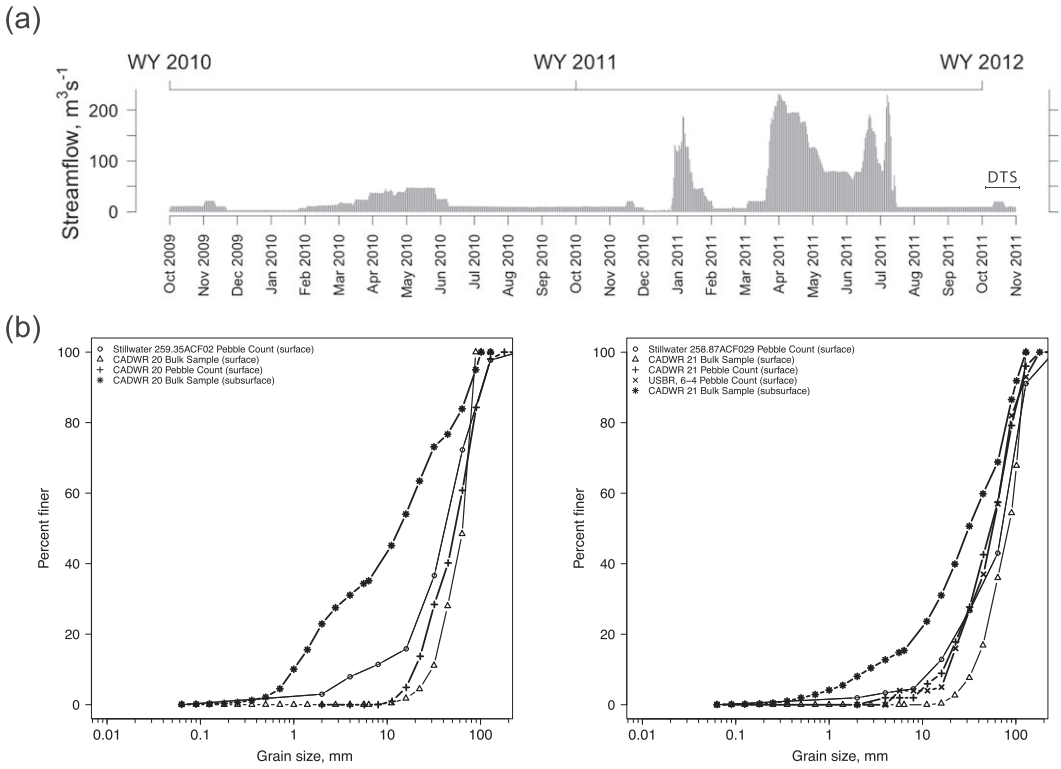


**Figure 3.** (a) Hydrograph for two-year period prior to and including the period of our field experiment. (b) Compilation of sediment grain size distribution data for Riffle 1 (left) and Riffle 2 (right) based on previously collected pebble counts, surface bulk samples, and subsurface bulk samples (US Bureau of Reclamation, 2014a).

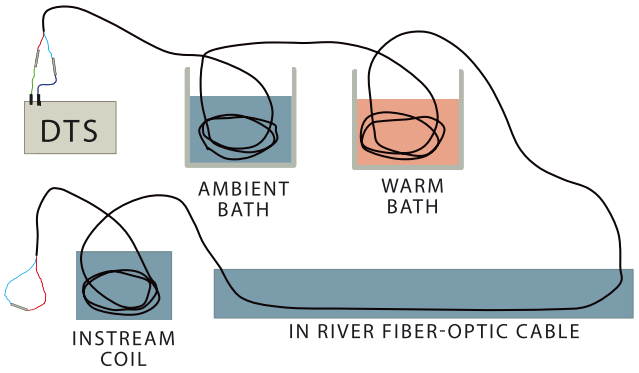


**Figure 4.** Configuration of fiber-optic distributed temperature sensing (DTS) cable installation and field reference sections of known and uniform temperature used for the purposes of calibration of near-bed temperatures. Reference sections were independently logged and sustained at a uniform temperature in the river installation. [Colour figure can be viewed at wileyonlinelibrary.com]

independently logged using two 100 Ω platinum resistance temperature detectors (PT100 RTD) (Thermoworks Inc., Lindon, UT, USA); (2) an ambient bath independently logged using two PT100 RTDs; (3) an *in situ* calibration coil along 20 m of the duplexed cable at the downstream end, independently logged using two HOBO® Water Temp Pro loggers (Onset Corporation, Bourne, MA, USA). Each of the PT100 RTDs was laboratory-calibrated against a NIST-traceable thermometer prior to installation.

During the installation, near-bed temperature data were collected at a spatial resolution of 2 m every five-minutes for 32 days of the controlled flow experiment (1.5 days at $10\,m^3\,s^{-1}$, 10 days at $20\,m^3\,s^{-1}$, 16 days at $10\,m^3\,s^{-1}$, and 4.5 days at 2–4 $m^3\,s^{-1}$) beginning on October 10, 2011 and ending on November 10, 2011. The DTS system collected measurements at a temporal scanning rate of 75 seconds for each of four fibers connected to the DTS unit, resulting in a temporal resolution of five minutes for each fiber. Throughout the installation, snorkel surveys were routinely conducted along the length of the reach to assess the presence or absence of sediment aggradation on top of the cable and to document any visible changes in the conditions of the streambed or the cable. Because the river is not wadeable at a $20\,m^3\,s^{-1}$ discharge, no snorkel surveys or measurements of sediment deposition were conducted during the 10-day period of the high flow.

After cable installation, the physical meter marks printed on the cable were surveyed with a global positioning system (GPS). While the physical meter marks on the cable do not correspond to the distances associated with the internal DTS measurements, they can be used together with the reference sections of uniform temperature when evaluating the data to identify specific locations along the cable and where it entered and exited the river channel. The stabilizing weights/stakes were still in place at the end of the flow experiment, indicating that the cable had not moved appreciably except in the downstream-most hundred meters of cable. In the segments that were buried with sediment during the higher flow, surveys of the total depth of sediment overlying the cable were conducted using a GPS, a gravelometer, and a ruler.

Three separate MATLAB® routines based on algorithms presented in (Hausner *et al.*, 2011) were used to calibrate the raw DTS data because these methods are more precise than the instrument-calibrated data, achieving precision of <0.1° root mean square error (RMSE). We used the calibration coil and two baths for reference sections all on the same side of the duplexed cable in the calibration. The accuracy and precision of the calibrated data are evaluated using independent temperature observations. We use the absolute mean bias of the calibrated data (Calibration Bias) and the RMSE (Calibration RMSE) as metrics for the quality of calibration for our raw data. The calibration results and accuracy of near-bed temperatures are shown in Table I.

## Bedload transport and disentrainment

Shear stress and sediment mobility calculations indicated no bedload transport occurred during the lower flows following the 10-day $20\,m^3\,s^{-1}$ discharge, and the temperature time series showed no evidence of systematic changes that would reflect any bed elevation changes. Thus, the depth of sediment deposition measured at the end of the 32-day installation was interpreted to be the same as at the end of the 10-day highest flow event. This depth, together with the $A_r$ and $\Delta\phi$ recorded at the last timestep of the high flow was then used in Equation (4) to calculate the $K_e$ value from the final burial depth for each location where the cable was buried. Then Equation (5) was used to calculate depths of sediment accumulation continuously over time, $\Delta z/\Delta t$, for the duration of the high flow. Temperature data from the first two days of the installation (October 10 and 11) were required to initialize the calculation of $\Delta z$, but because the high flow pulse did not begin until around noon on October 11, only half of one day of potential bed changes are unreported by the analysis.

Boundary shear stress $\tau$, depth, velocity and water surface elevation along the study reach were predicted using a previously validated two-dimensional hydraulic model (SRH-2D) (US Bureau of Reclamation, 2008, 2014b) for two constant discharges: the same $20\,m^3\,s^{-1}$ (Q1.5) constant-intensity discharge during which we observed sediment mobility, and a hypothetical $217\,m^3\,s^{-1}$ (seven-year flood, Q7) flow event. The second, higher flow event was simulated primarily to aid in the interpretation of our field observations and to assess the sediment transport potential and functioning of the riffle-pool reaches. For additional detail regarding the SRH-2D model used here, including its original development and validation, the interested reader is referred to US Bureau of Reclamation (2014b).

The thalweg was digitized using ArcGIS by identifying the minimum elevation at each cross-section within the 2D bathymetry mesh, and adjusting selected thalweg points where necessary in order to ensure a continuous line. The distance along the thalweg was computed using the 'Near' geoprocessing tool in ArcGIS. The water surface slope was then calculated along the thalweg based on the water surface elevations predicted in SRH-2D and the distance between the centroid of each model grid node. This average cross-section slope was used in all transport calculations.

Bedload transport rates, $q_s$, were computed for each of the two discharges for (1) the length of the thalweg, and (2) the entire extent of the 2-km reach using three bedload transport equations. Full details of the bedload formulae used here can be found in the original references (Meyer-Peter and Müller, 1948; Wilcock and Crowe, 2003; Singer and Dunne, 2004). With the exception of Meyer-Peter and Müller (1948) which uses a single grain size, the full bed material grain size distribution was used and fractional bedload transport rates were computed for each grain size class. In order to focus on the differences in transport in distinct portions of the reach, we selected the grain size distribution taken from a bulk sample at the head of Riffle 1 with a median particle size of 64 mm, and applied this grain size distribution to the entire reach for all transport calculations. Maps of the predicted sediment

**Table I.** Calibration metrics for the field deployment of fiber optic distributed temperature sensing (DTS) cable

| | 1300-m fiber optic cable DTS channel 1 and 2 | 700-m fiber optic cable DTS channel 3 and 4 |
|---|---|---|
| **Calibration and validation sections** | Warm bath (1st pass)<br>Ambient bath (1st pass)<br>Calibration coil (Hobo 3, 1st pass)<br>Warm bath (2nd pass) | Warm Bath (1st pass)<br>Ambient Bath (1st pass)<br>Calibration Coil (Hobo 2, 1st pass)<br>Warm Bath (2nd pass) |
| **MATLAB indices of reference sections** | [7 11;17 23;601 610]<br>valid = 1305:1308<br>step index = 657 | [9 13;20 24;355 357]<br>valid = 716:720<br>step index = 366 |
| **Calibration RMSE (°C)** | 0.068 ± 0.012<br>(0.029 to 0.118) | 0.071 ± 0.053<br>(0.015 to 0.329) |
| **Calibration Bias (°C)** | 1.63e-05 ± 5.63e-06<br>(2.88e-06 to 4.75e-05) | 2.697e-05 ± 5.486e-05<br>(7.400e-07 to 0.0004) |
| **Validation RMSE (°C)** | 0.923 ± 0.597<br>0.034 to 3.255 | 1.165 ± 0.842<br>(0.024 to 4.504) |
| **Validation Bias (°C)** | −0.867 ± 0.663<br>(−3.250 to 1.007) | −0.753 ± 1.222<br>(−0.0007 to −4.503) |
| **Duplex Check (°C)** | Mean offset = 0.434<br>Standard offset = 0.487 | Mean offset = 1.190<br>Standard offset = 2.566 |

Note: The use of reference sections along the 2-km cable (rather than individual points) is intended to minimize the uncertainty of the temperatures on which the calibration is based. The installation recorded data at 2 m spatial sampling interval, 75 second integration times, totaling measurement records at five-minute intervals sampled every 2 m over the length of the 2-km cable. These measurements were recorded continuously for the 32-day installation period. The number of points used in each reference section varied and is shown with the numbered MATLAB indices. Root mean square error (RMSE) and Bias for both the validation and calibration baths are reported as the mean ± the standard deviation of field traces. The duplexing error is not specific to the calibration or validation baths, and is reported once for each calibration algorithm as the mean ± the standard deviation of the total number of traces. Details on the calibration routines employed herein are presented in Hausner *et al.* (2011).

transport rates based on various formulae were developed to illustrate the magnitude and spatial pattern of the bed mobility.

## Results

### Near-bed temperature and sediment accumulation

The degree to which near-bed temperatures change as a result of sediment deposition is shown graphically in Figure 5 by the lines plotted for each 2-m cable segment at a location in Riffle 2. At the segments plotted in Figure 5, the cable was buried by sand in a plume downstream of a mid-channel bar. At the beginning of the experiment (October 10, 2011), all locations along the length of the DTS cable had consistent, diurnal temperature variations. Within the first few days of the onset of the 20 $m^3 s^{-1}$ flow, the daily temperature variations at some locations on the cable became buffered and lagged to varying degrees due to the fact that sediment was gradually burying the cable. This can be seen by comparing the blue line showing

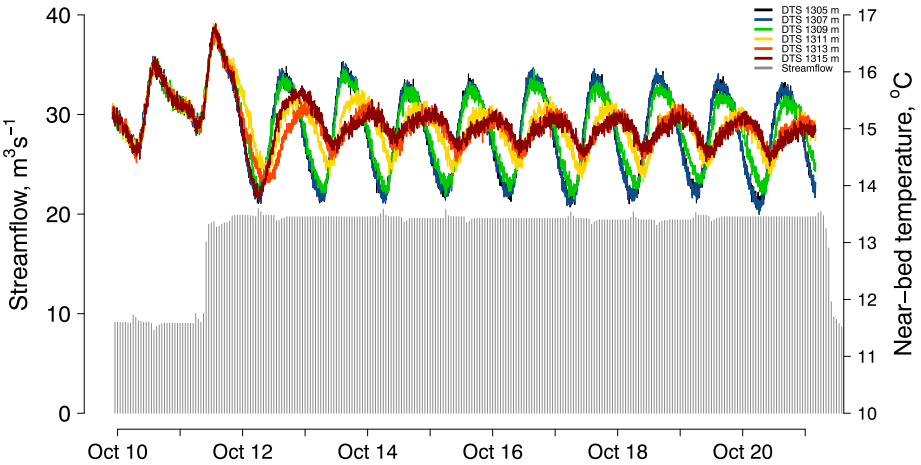


**Figure 5.** Sediment deposition, recorded via near-bed temperature time series and validated with observations, coinciding with bar evolution during 32 days of ongoing experimental restoration flow releases in the San Joaquin River downstream of Friant Dam. Near-bed temperature time series (colored lines) are overlaid upon the flow hydrograph (gray bars), comprised of a 10-day minor flood pulse during which the bed became mobile. Each colored line represents a temperature record measured by the distributed temperature sensing (DTS) cable at different distances downstream from the tail of a gravel bar where a plume of sand was gradually deposited. Here, there are two phenomena that are convolved: (1) the dampening of the amplitude and the lagging of the phase at locations where the cable was gradually buried by sediment; (2) the diurnal variability in the temperature of the water, so there would be temporal variability in the temperature, even if there was no deposition. Together these combine to produce lines representing the surface water temperature (i.e. DTS 1305) and the gradual transition to subsurface temperature (i.e. DTS 1315). [Colour figure can be viewed at wileyonlinelibrary.com]

the temperature at a bar location that was free of sediment deposition, and the red line showing temperature at the downstream end of the bar where mainly sand buried the cable. The gradual changes in $A_r$ and $\Delta\phi$ (Equations (1) and (2)) were then interpreted as resulting from gradual aggradation over the course of the Q1.5 flood.

Post-flood snorkel surveys and bed sediment measurements during cable removal indicated that two fractions of sediment were mobile in narrow active zones alongstream during the Q1.5 – sand and gravel – as well as large woody debris. The snorkel surveys indicated a consistent spatial pattern among the deposition zones. Gravel accumulated on bar tops and tails (on the lee face), while sand accumulated in long plumes immediately downstream of the gravel bar tails (Figure 6). The deposited gravel layer consisted of coarse gravel with some cobbles (> 90 mm) embedded in the fresh matrix overlying the cable, suggesting that in these areas a coarse surface layer was maintained despite the mobility. At the end of the entire 32-day flow experiment, as the cable was retrieved, it was discovered that the lowering of the amplitude ratio and increase in the phase lag of the temperature signals had occurred only at locations where the cable was buried by sediment along bar tops and tails, whereas the cable that remained on the surface, free of sediment (indicating either scour or no change in bed elevation), measured temperature signals that had not changed.

Gravel deposition (Figure 7a) predominantly occurred on bar tops and tails (e.g. Figure 6) and resulted in a near-bed temperature signal that is less buffered and lagged than that of sand deposition. The near-bed temperature amplitude decrease and phase shifts differed between zones of predominantly gravel deposition and predominantly sand deposition. The sinusoidal temperature time series changes more dramatically in zones of sand deposition (Figure 5). In contrast, Figure 7b shows that changes to the diurnal temperature signal are apparent but less pronounced along zones where we observed up to 30 cm of coarse gravel deposition, as was the case along the top and the lee of the bar on Riffle 1 (Figure 7a).

From those temperature changes, we can quantify the onset, end point, and rate of change of disentrainment and compute the resulting changes in streambed elevation, $\Delta z$, continuously over distance and time. Here we pay detailed attention to the zones of gravel deposition due to the role of gravel transport in shaping bars and its ecological importance. Figures 8 and 9 show the change in bed elevation resulting from gravel deposition over time at different distances along bar tops and tails in Riffle 1 and Riffle 2, respectively. The black line in both Figures 8 and 9 indicates the total depth of sediment that was measured at each distance along the buried cable segment at the end of the experiment. Temperature data from the first two days of the installation (October 10 and 11) were required to initialize the calculation of $\Delta z$, but because the high flow pulse did not begin until around noon on October 11, only half of one day of potential bed changes are missed.

The conclusions we can make from the gravel deposition results plotted in Figures 8 and 9, shown in the corresponding photographs, and indicated by measurements of fill thickness over the cable at the end of the field experiment are as follows. First, there was sediment motion during a constant-intensity flow of 20 $m^3 s^{-1}$ with a recurrence interval of 1.5 years. The minor flood pulse locally mobilized sediment in narrow, active zones of transport in the streamwise direction, with gravel disentrainment observed over tens of meters of the entire cable. Second, all grain sizes in the bed material (up to 128 mm) were burying the cable in gravel deposition zones, which implies that the Q1.5 flow was sufficient to mobilize entrainable grains. Third, approximately 20–30 cm of gravel (~3–5 times $D_{50}$) accumulated on the lee sides of the bars. Fourth, the rate of change in bed elevation over time was not constant during the constant-intensity minor flood pulse. Last, the bedload regime alternated between erosion and deposition at a given location during a single constant flow event.

By the end of the third day of steady flow, there was evidence of motion at the locations shown in Figures 8 and 9 for deposition zones along Riffle 1 and 2, respectively. At that time, accumulation of sediment was observed at all distances plotted, resulting in net positive bed elevation changes by the end of the 10 days. This deposition was confirmed at the end of the experiment by our field measurements as illustrated in the corresponding photographs at each of the two riffles. At the onset of the Q1.5, Figures 8 and 9 suggest that no deposition was occurring in the first two days. The missing

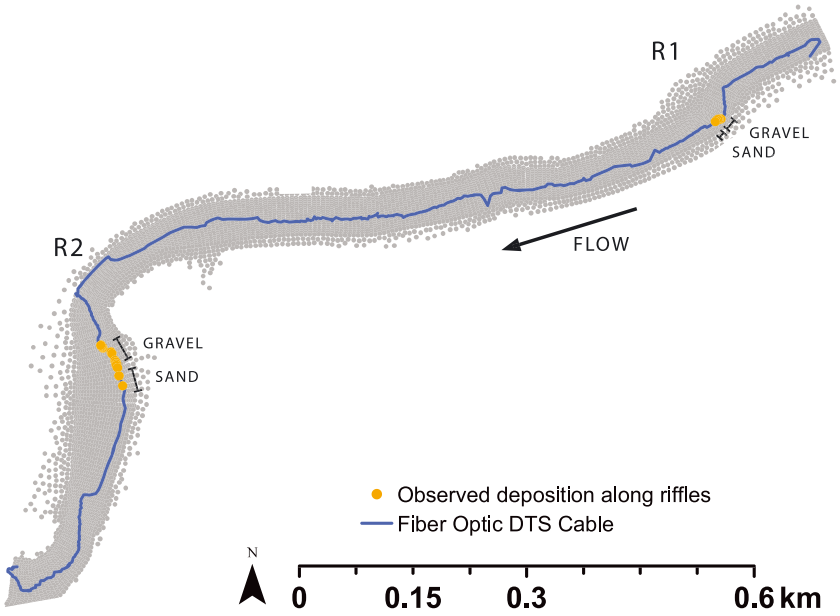


**Figure 6.** Observed zones of sediment deposition in Riffles 1 and 2 (R1 and R2) along the distributed temperature sensing (DTS) cable, as indicated by post-flood snorkel surveys using a global positioning system (GPS) and bed sediment measurements during cable removal. Gravel accumulated on bar tops and tails (on the lee face), while sand accumulated in short or long plumes immediately downstream of the gravel bar tails. [Colour figure can be viewed at wileyonlinelibrary.com]

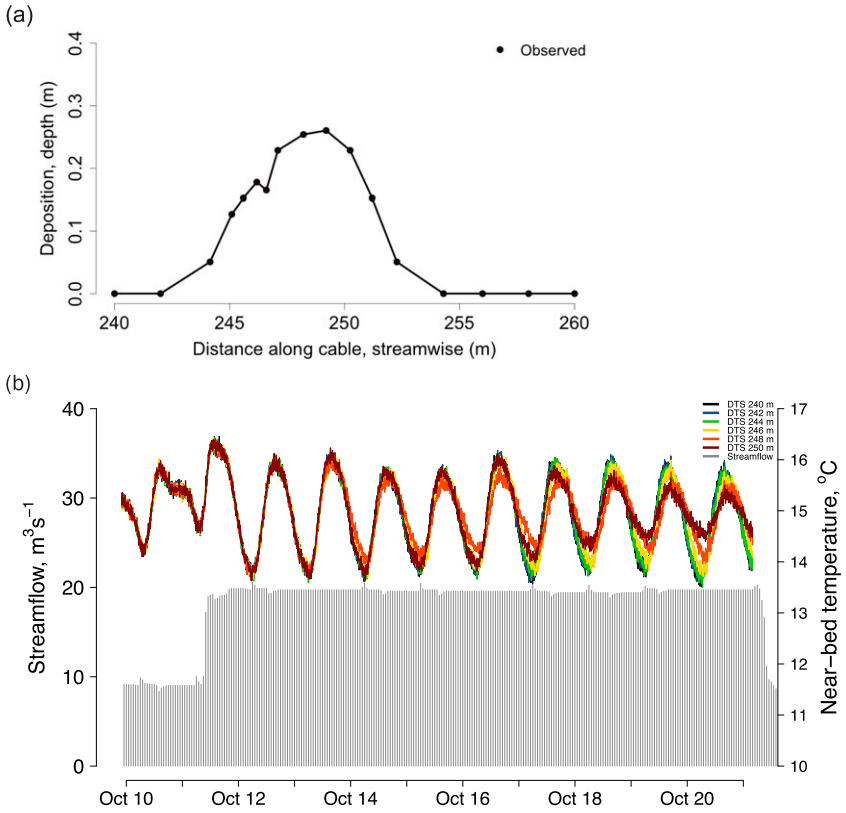


**Figure 7.** Observed gravel deposition over the length of a gravel bar during a 1.5-year flood (Q1.5) (20 $m^3\ s^{-1}$) from October 11 to October 21 in the San Joaquin River, CA, USA. (a) Total sediment deposition that occurred at Riffle 1 during a 10-day pulse flow event. Distances over the length of the bar are approximate and correspond to the second of two consecutive bars. (b) Temperature time series during a 10-day minor flood pulse corresponding to the deposition plotted in (a). The deposition plotted in (a) was observed along the lobe front of the second consecutive bar in the upstream-most riffle of the 2-km study reach ('Riffle 1'). Deposition increased over the length of the bar (distance), with the greatest deposition occurring along the steepest lee face of the bar. [Colour figure can be viewed at wileyonlinelibrary.com]

points indicate that either $\Delta z$ was zero, which means that the cable was exposed to water and not buried, or that there was scour. Because our installation did not include a deeper, second temperature sensor, we cannot verify whether or not scour was occurring.

Local-scale variations in the rate of disentrainment over time are also shown by the time series of changes in streambed elevation, $\Delta z$, in Figures 8 and 9 in both Riffle 1 and Riffle 2, respectively. We are able to see centimeter-scale changes in bed elevation over time, $\Delta z/\Delta t$, which varied through time during the constant discharge. There were also differences in the timing of the most rapid changes in bed elevation occurring during the course of the constant flood pulse (Figures 8 and 9). For example, in some bar locations the greatest changes occurred within the first 3–4 days of deposition, whereas in other locations the greatest changes occurred over the last two days of the flow event. Our interpretation of this result is that either the sediment supply was exhausted before the end of the flow pulse, or the locus of deposition changed to zones not recorded by the DTS cable.

## Sediment mobility and transport rate

The Shields criterion was used to assess the predictability of the observed sediment motion for the Q1.5:

$$\tau_c^* = \frac{\tau}{(s-1)\rho g D_{50}} \tag{6}$$

where $\tau_c^*$ is the dimensionless critical shear stress, $\tau$ is the bed shear stress, $g$ is the acceleration of gravity (9.81 m $s^{-2}$), $\rho$ is water density (1000 kg $m^{-3}$), and $s = \rho_s/\rho = 2.65$. Shear stresses along the reach were calculated using an existing 2D flow model (US Bureau of Reclamation, 2014b). When we employ a median grain size of 64 mm from a representative bulk sample from Riffle 1, we find that the onset of motion is consistent with a $\tau_c^*$ of 0.02 to 0.03 for the Q1.5. This assertion is supported by other compilations and relations of $\tau_c^*$ values versus slope suggesting that it is reasonable to believe it is less than 0.03 (Lamb *et al.*, 2008; Mueller *et al.*, 2005).

Figure 10 indicates that $\tau$ along the channel thalweg varies from less than 1 to 74 N $m^{-2}$ during the Q1.5, with the highest values on the riffles and low values in the long pools and runs. The modeled Q7 produced values of $\tau$ varying from 7 to 90 N $m^{-2}$ along the thalweg of both the riffles and the long pools and runs. To examine the spatial extent and continuity of an index of bed mobility, transport rates along the thalweg were calculated using Meyer-Peter and Müller (1948) for both discharge events using a $\tau_c^*$ of 0.047 and the single median grain size (64 mm) that is representative of some gravel particles observed in depositional zones during our field experiment. Figure 10 shows that at some places along the thalweg transport was predicted during the Q1.5 discharge, which is supported by the DTS records indicating that there was some mobility in proximity to the cable. The distance along the thalweg over which transport rates were positive for the Q1.5 event is limited to tens of meters over the riffles where $\tau$ is sufficiently high, and extends to a slightly larger proportion of the thalweg at the Q7 discharge. More important is the fact that, in either discharge event, transport was not predicted to extend continuously through the pools.

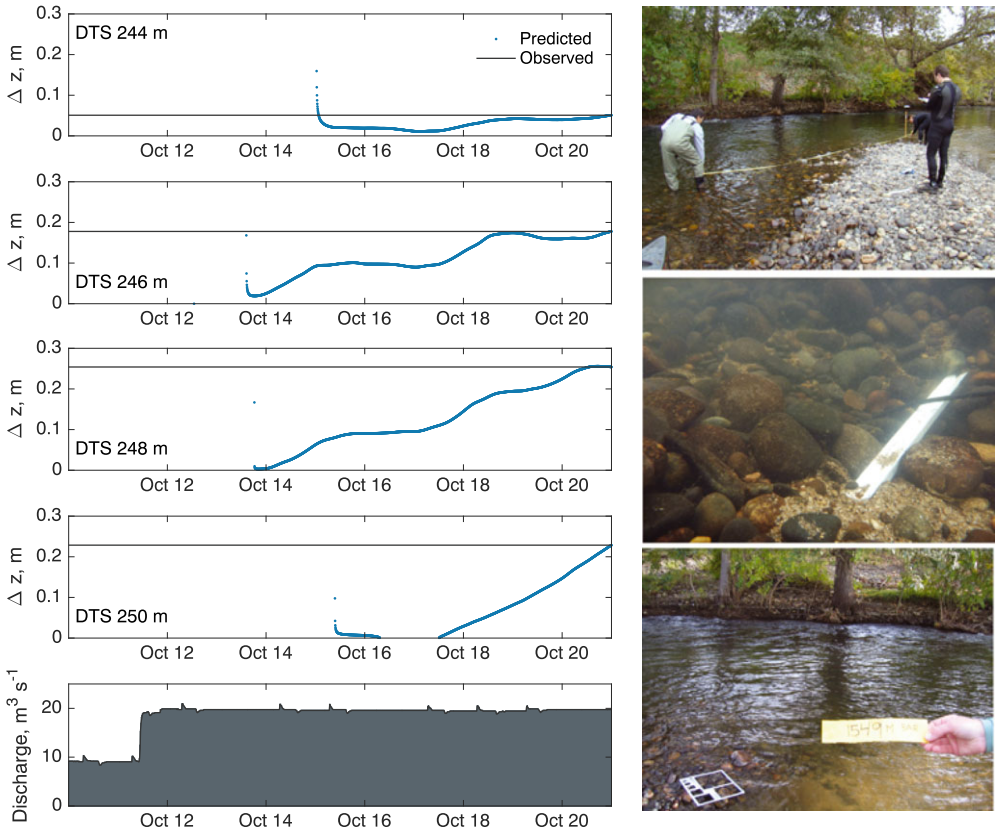


**Figure 8.** Gravel bar evolution during a 10-day sediment mobilizing flow (Riffle 1). Shown are changes in bed elevation continuously over time during a constant 10-day flood event ($20\,m^3\,s^{-1}$) from October 11 to October 21 in Riffle 1 of the study site on the San Joaquin River, CA, USA. Deposition is predicted at 2-m intervals over the length of a gravel bar. Deposition rates were validated using point measurements of the depth of sediment deposition at the end of the experiment in the locations where the fiber-optic distributed temperature sensing (DTS) cable had been buried by gravel. [Colour figure can be viewed at wileyonlinelibrary.com]

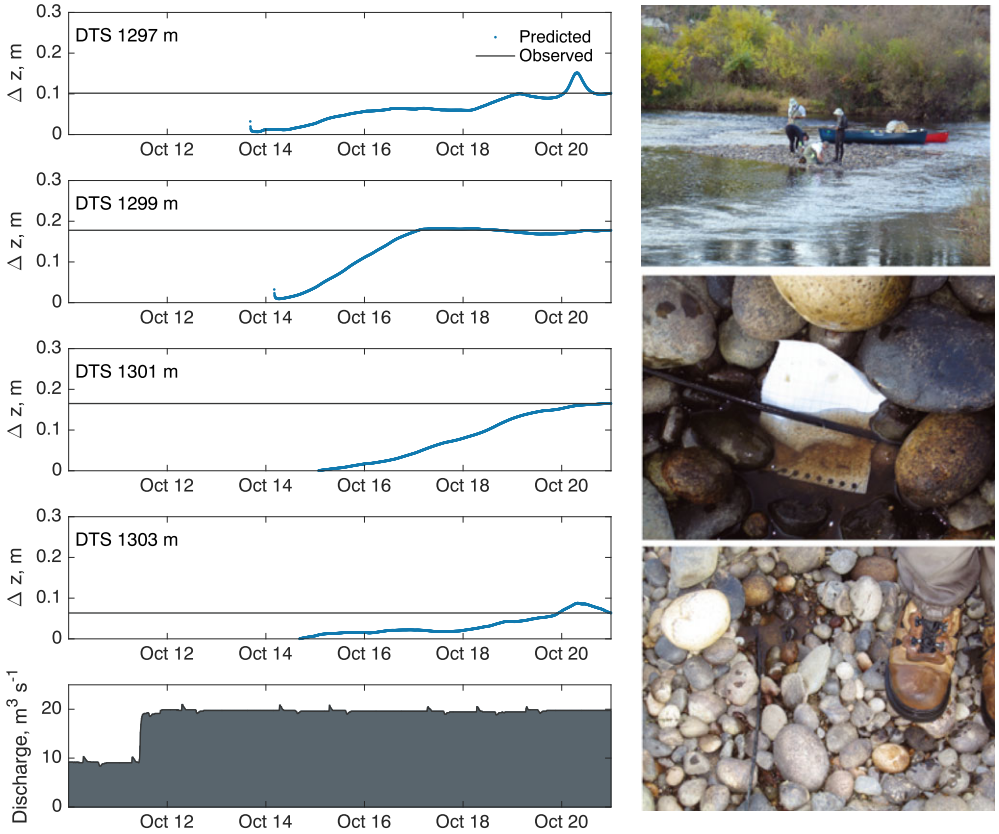


**Figure 9.** Gravel bar evolution during a 10-day sediment mobilizing flow (Riffle 2). Shown are changes in bed elevation continuously over time during a constant 10-day flood event ($20\,m^3\,s^{-1}$) from October 11 to October 21 in Riffle 2 of the study site on the San Joaquin River, CA, USA. [Colour figure can be viewed at wileyonlinelibrary.com]

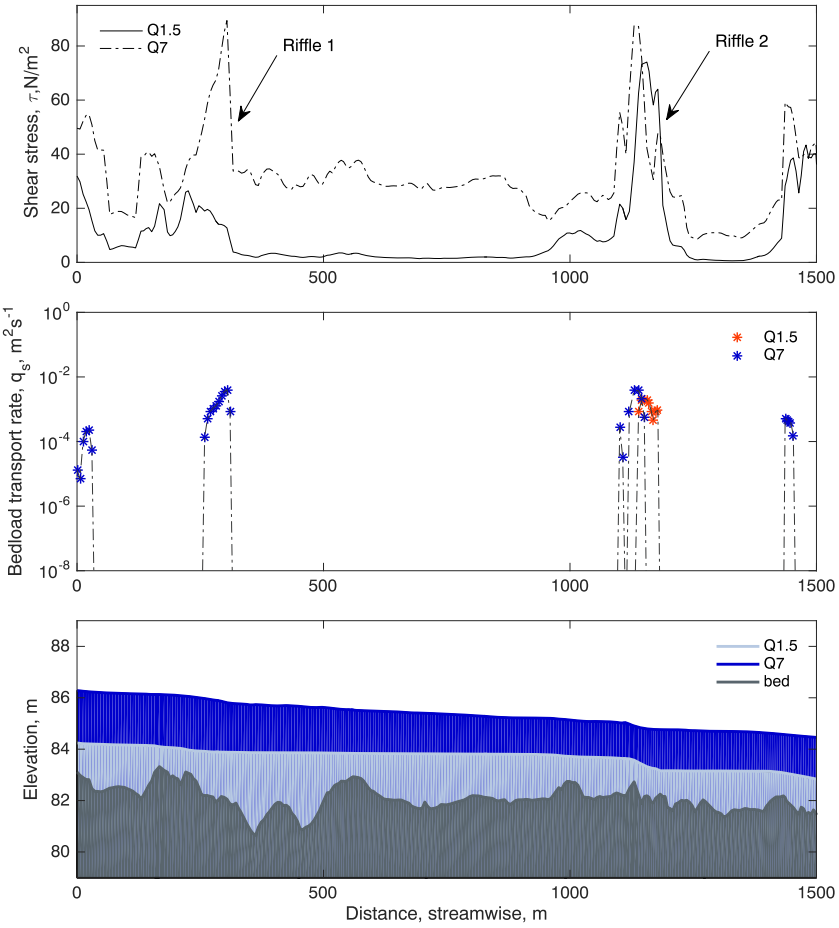


**Figure 10.** Thalweg profile of shear stress and predicted thalweg bedload transport rates for two constant discharge events (20 and 217 $m^3 s^{-1}$) for a single grain size ($D_{50}$ = 64 mm). Shown in the middle panel are transport rates along the thalweg based on Meyer-Peter and Müller (1948) corresponding to the constant 1.5-year flood (Q1.5) and seven-year flood (Q7) events over the length of reach where sediment deposition was observed. The corresponding water surface and bed elevation along the thalweg profile are shown in the lower panel. Predicted transport rates corroborate our observations that gravel transport was restricted to short zones over the riffles during the Q1.5 event. [Colour figure can be viewed at wileyonlinelibrary.com]

In order to elucidate the morphologic functioning of these sediment starved riffle-pool reaches, three bedload equations were used to predict sediment transport rates for the full 2D extent of the reach (Meyer-Peter and Müller, 1948; Wilcock and Crowe, 2003; Singer and Dunne, 2004). Figure 11 shows the spatial patterns of bedload transport potential superimposed on the planform using different formulae for the observed Q1.5 (left panel) and hypothetical Q7 (right panel) discharge events. The Meyer-Peter and Müller (1948) equation with a $\tau_c^*$ of 0.047 fails to predict sediment mobility during a Q1.5 flow in each of the zones where we observed deposition (Figure 6). However, when we adjust $\tau_c^*$ to 0.02 (Figure 11b), we can correctly predict the spatial patterns of what we observed, which is that small amounts of the coarse bed material moved in and around an otherwise immobile bed and intact armor layer. Insertion of a $\tau_c^*$ to 0.02 of course predicts more extensive transport consistent with the locations of the recorded deposition (Figure 6), but distorts the magnitude of predicted transport because the coefficients of the original equation were calibrated with the larger $\tau_c^*$ value. While we recognize that lowering $\tau_c^*$ will yield transport rates that are somewhat biased, the assumption of a lower $\tau_c^*$ is consistent with measurements of sediment mobility in low gradient rivers (Lamb *et al.*, 2008; Mueller *et al.*, 2005) similar to that of our study site.

The predictions following the modified Meyer-Peter and Müller (1948) (Figure 11b), Singer and Dunne (2004) (Figure 11c), and Wilcock and Crowe (2003) (Figure 11d) formulae yield sediment transport rates that vary in magnitude, but all three suggest a consistent spatial pattern during the Q1.5, which is that active zones of transport mainly occurred on bar surfaces along sections that were tens of meters in length with 3–6% of the bed predicted to be mobile (Figures 11b–11d, Table II). The Singer and Dunne (2004) and Wilcock and Crowe (2003) equations both generally indicated positive rates of transport when $\tau$ exceeds ~10 N $m^{-2}$, with a wider range of transport rates predicted by Wilcock and Crowe (2003). This is attributed to the fact that the Singer and Dunne formulae computes fractional transport specific to the shear stress of a particular particle size once the whole bed mixture has reached a previously defined threshold. In this case, the excess shear stress is defined using the $D_{50}$ particle size rather than the grain size class of interest, similar to the Meyer-Peter and Muller equation. The Wilcock and Crowe equations instead define a dimensionless reference shear stress for the geometric mean particle size on the bed surface as a function of the fraction of sand on the bed surface. Distinct zones of mobility spanning areas on the order of tens of meters in length are predicted by all of the equations with no mobility occurring through the long pools. Within these narrow active zones, the transport rates generally range from $10^{-6}$ to 0.1 kg $m^{-1} s^{-1}$ corresponding to shear stresses in the range 20–90 N $m^{-2}$. More important than the precise magnitude of any one prediction is that all three formulae demonstrate a consistent pattern, which is that the predicted transport rates vary spatially by many orders of

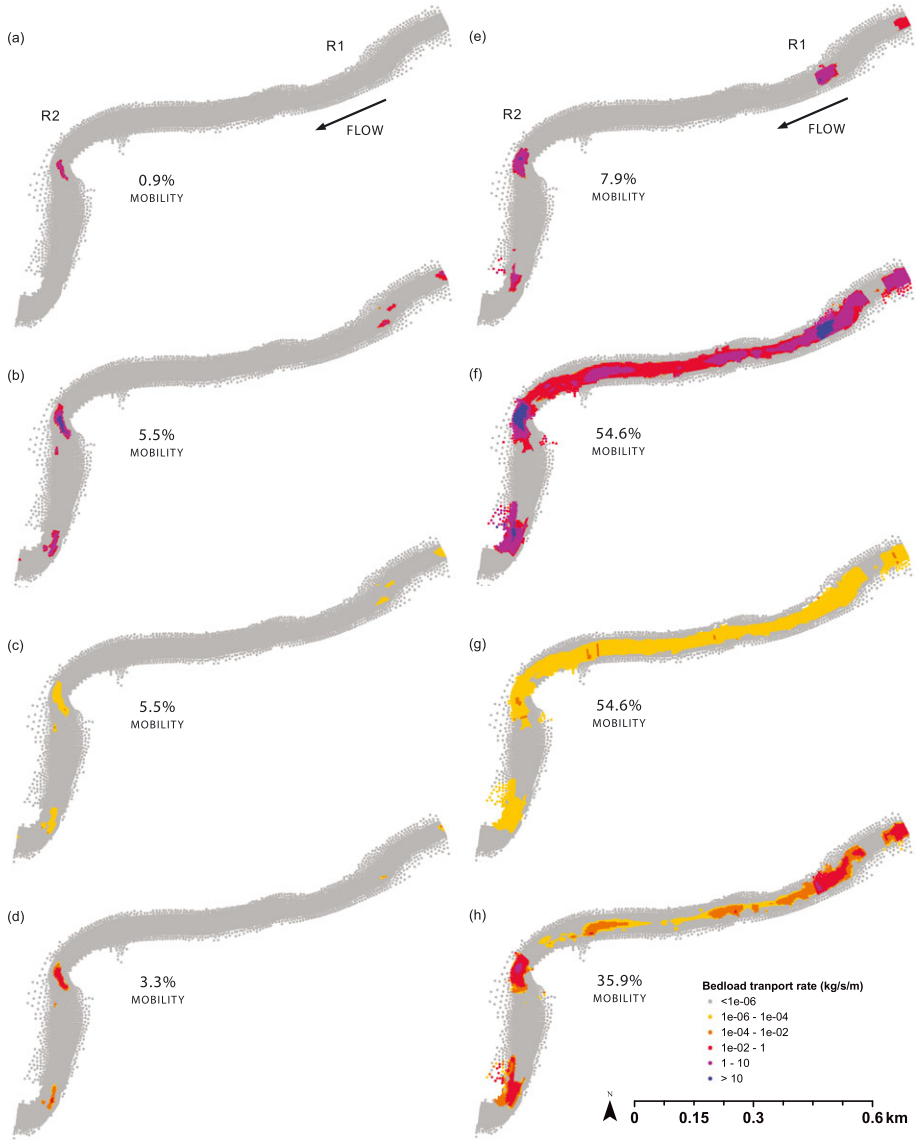


**Figure 11.** Spatial pattern of bedload transport rates predicted for two constant discharge events using three different formulae. Predictions corresponding to the 20 $m^3 s^{-1}$ flow event (1.5-year flood, Q1.5) include (a) traditional Meyer-Peter and Müller (1948) using a $\tau_c^*$ of 0.047, (b) modified Meyer-Peter and Müller (1948) using a $\tau_c^*$ of 0.02, (c) Singer and Dunne (2004), and (d) Wilcock and Crowe (2003). Predictions corresponding to the 217 $m^3 s^{-1}$ flow event (seven-year flood, Q7) include (e) traditional Meyer-Peter and Müller (1948), (f) modified Meyer-Peter and Müller (1948), (g) Singer and Dunne (2004), and (h) Wilcock and Crowe (2003). Shear stress values corresponding to each flow were obtained from two-dimensional (2D) hydraulic modeling and an observed grain size distribution with a median grain size of 64 mm was used in the transport calculations. Colors denote the bedload transport rates in kg $m^{-1} s^{-1}$. [Colour figure can be viewed at wileyonlinelibrary.com]

magnitude and are limited to fractions of the length and width of the reach during the observed Q1.5 event, with transport confined to the riffle and absent through the long pools.

As flow increases, inactive zones through the pools and runs are replaced by zones of partial or nearly complete transport during the Q7 (Figures 11e–11h). The traditional equation of

**Table II.** Proportion of the bed that was predicted to be mobile and inactive during two different discharges, including a flood with a recurrence interval of approximately 1.5 years (20 $m^3 s^{-1}$) and a flood with a recurrence interval of approximately seven years (217 $m^3 s^{-1}$)

| | Q1.5 20 $m^3 s^{-1}$ (700 cfs) | | Q7 217 $m^3 s^{-1}$ (7650 cfs) | |
|---|---|---|---|---|
| | Partial mobility | Inactive | Partial mobility | Inactive |
| Meyer-Peter and Muller (1948) | 0.9% | 99.1% | 7.9% | 92.1% |
| Meyer-Peter and Muller (1948) (adjusted $\tau_c^*$) | 5.5% | 94.5% | 54.6% | 45.4% |
| Singer and Dunne (2004) | 5.5% | 94.5% | 54.6% | 45.4% |
| Wilcock and Crowe (2003) | 3.3% | 96.7% | 35.9% | 64.1% |

Note: Bedload transport was calculated using three different formulae (Meyer-Peter and Müller [1948], Singer and Dunne [2004], and Wilcock and Crowe [2003]). Meyer-Peter and Müller equation was calculated assuming a $\tau_c^*$ value of 0.047 and an adjusted value of 0.02.

Meyer-Peter and Müller (1948) indicates that little to no transport occurs (Figure 11e), but once adjusted it indicates that the threshold of motion during the Q7 is exceeded along 55% of the reach (Figure 11f). The fractional transport formulae of Singer and Dunne (2004) (Figure 11g) and Wilcock and Crowe (2003) (Figure 11h) also predict mobility occurring in 55 and 36% of the reach, respectively. All formulae predict that the Q7 event would also be unable to transport sediment through the long, deep pool at the downstream-most end of the reach. While partial mobility occupies a much larger proportion of the bed during a Q7 in both formulae, the spatial patterns of the inactive zones differ only slightly and highlight the occurrence of an extensive immobile pool zone through which sediment is not likely to be transported in the analyzed range of flows. Thus, transport is predicted along the riffles in relatively narrow zones that are flanked by an otherwise inactive bed, even at the much higher flow.

Because bedload rates were not directly measured in this study, it matters less which equation is used as none of the equations were calibrated to match this particular river system. The utility of the equations here is in their ability to elucidate the spatial patterns of transport along the reach in order to discriminate between the function of a full-mobility event versus a partial mobility event and during the initial phase of transport. We can correctly predict that transport occurs along the riffles for a Q1.5 during which we observed mobility of coarse sediment, albeit at relatively low rates. More important than the performance or exact magnitude predicted by any single formulae is the indication that the Q1.5 is sufficient to locally disturb and transport gravel along the riffles in areas covering tens of meters, but in no formulae is it sufficient to generate whole-bed transport continuously through the long pools. This is supported by our observations, which indicated that gravel disentrainment was restricted to the riffles and not in the pools.

## Discussion

Near-bed temperature measurements and calculations of disentrainment, and sediment transport theory indicate that (1) coarse and fine sediment was mobilized during a Q1.5, (2) mobility was limited to narrow active zones of transport along the riffle complexes, (3) the ensemble of mobile grains were most likely sourced from partially- or fully-mobile source areas within the riffle along an otherwise immobile and relatively stable bed, and (4) transport distance was likely to be relatively short and on the order of sub-meter to meter length scales.

We calculated the spatial patterns of the bedload flux rates, $q_s$, to illustrate how the pattern of bed mobility would be extended during the higher flow event. We used three transport equations to obtain indices of bedload transport intensity as the flux rates: one equation employed a single grain size and was flume-calibrated on sediment significantly finer-grained than the San Joaquin (Meyer-Peter and Müller, 1948); the second equation was field-calibrated using particle sizes in the lower range of the San Joaquin, incorporated grain size sorting and hiding, but was calibrated for high rates of sediment transport (Singer and Dunne, 2004); the third equation was flume-calibrated, accounts for hiding, and explicitly references the sand content of the bed as a driving variable (Wilcock and Crowe, 2003).

We have predictions and field documentation of localized sediment mobility during a Q1.5 corresponding to approximately half of the bankfull flow. This raises an important geomorphic question regarding the spatial discontinuity of between-riffle transport which is required in order to maintain the relief of the bar features and to keep the deep pools free from filling in with sediment. The map indices demonstrate that greater spatial continuity of transport could be expected at Q7 and higher. However, calculations of transport capacity do not take into account the effects of sediment supply exhaustion, or of bed coarsening, and therefore the patterns in Figure 11 are an insufficient basis for concluding whether or not the time-integrated transport capacity through the pools will be sufficient to accommodate all the sediment eroded past the riffles.

Perhaps the more important aspect of the bedload predictions in Figure 11 is in the distinction between localized transport during texture-forming and bar-growing flows (Q1.5), and partial- to whole-bed transport during flushing and channel-forming flows (Q7). In the absence of field data during the higher flow event, the predictions corroborate our understanding that the transport of coarse sediment from one riffle downstream to the next and the maintenance of the riffle and pool morphology occurs relatively infrequently. The results provide a mechanistic basis to explain from where and at what rate the observed, mobile sediment was transported, but further investigation is needed to understand (1) under what conditions are the pools being flushed and riffles being maintained over decadal and longer time periods, and (2) what is the relationship, if any, between the rate of entrainment and the rate of disentrainment, the latter of which was the focus of our study. Additional studies with DTS technology could aid in understanding and distinguishing between 'flushing flows' (Kondolf and Wilcock, 1996) and texture-forming and bar-growing flows, and in determining whether observed changes in bed elevation contribute to bar maintenance over decadal timescales, or whether the bars are elongating or gradually filling in the pools.

Use of near-bed temperature time series can quantify deposition at the scale of centimeters during a minor pulse flow event. The technology facilitates measurements of critical fine-scale processes that cannot be made using most other field methods. While the magnitude and rate of transport and deposition assessed here are modest for morphologically-significant flows in gravel bed rivers, previous studies have shown that substantial transport rates of all grain sizes found on the bed surface can occur when the bed is only partially mobile (Wilcock and McArdell, 1997). Our analysis demonstrates that disentrainment and bed elevation changes generated at frequent recurrence intervals (i.e. 1.5 years) – that may have otherwise been left undetected by topographic surveys, scour chains, or point-based samplers – may be quantified and interpreted spatially with modeling.

The method and analysis has further potential to aid in understanding the fine-scale mechanics of gravel bar evolution. This resolution of detection of channel change, for example, would not have been possible through traditional survey or remote sensing methods, therefore field detection of the onset of motion may have been missed. With careful deployment, the methods introduced here may also be useful in testing predictions of channel scour and/or deposition resulting from larger flows than those considered here or over a period of years. Future improvements to further validate and support the method include: (1) measurements of the deposition depth overlying the cable during the flood to confirm validity of the $K_e$ value calculated from measurements of burial depth after the flood; (2) measurements of temperature along the bed surface and at a second depth in the bed in order to measure both scour and fill; (3) measurements of temperature both longitudinally and cross-sectionally to record deposition over a greater extent of the reach; (4) measurements of localized grain size distributions in anticipated zones of mobility before and after the sediment-mobilizing flow (though doing so may cause disturbance to the bed); and (5) direct measurements of bedload transport rates

to corroborate measurements of $\Delta z/\Delta t$ and to calibrate sediment transport formulae for subsequent analysis.

Several potential sources of error can make the comparison between the internal DTS distances and those physical meter marks printed on the cable imprecise, which will require detailed GPS surveys before and after high flows in installations of longer duration. With supplemental measurements in addition to those presented here, it may be feasible to evaluate more closely a single particle moving out of its pocket as indicated by a time series that alternates between deposition and erosion on the scale of centimeters. The method has the potential to aid in the design and implementation of river habitat restoration strategies (e.g. flow manipulation, gravel augmentation), which generally requires a prediction of morphologic changes at both fine timescales when the bed texture matters to gravel-spawning fish and coarse timescales when the bar forms, migration, and pool maintenance matter to channel evolution processes influencing habitat features such as depth and velocity in pools and runs.

*Acknowledgements*—This work was supported by the California Delta Stewardship Council Delta Science Program under Award Numbers U-04-SC-005 and U-05-SC-058, and an Instrumentation Grant from the Center for Transformative Environmental Monitoring Programs (CTEMPS). The authors thank field assistants Eric Fournier, Kyongho Son, Oliver Soong, Kevin Huniu, Andrew Hafs, and Aubrey Dugger, in addition to Richard Sloan and Chuck Kroeger of the RiverTree Volunteers for their provision of canoes and field support. The authors thank Elaina Gordon and Katrina Harrison at the US Bureau of Reclamation for their data provision. Michael Singer and Daniele Tonina provided helpful suggestions on computations. The authors thank three anonymous reviewers for their insightful comments that helped improve the paper. Data used in this article can be obtained from the lead author.

## References

Andrews E. 1994. Marginal bed load transport in a gravel bed stream, Sagehen Creek, California. *Water Resources Research* **30**(7): 2241–2250.

California Department of Water Resources. 2010. *CDWR 2009 Interim Flows Data Report DRAFT, 3/26/2010. Appendix IV: 34 San Joaquin River Riffle Particle Size Composition Survey Interim Report, River Miles 247–267*, Final Draft. California Department of Water Resources: Sacramento, CA.

Chung C-C, Lin C-P. 2011. High concentration suspended sediment measurements using time domain reflectometry. *Journal of Hydrology* **401**(1): 134–144.

Chung C-C, Lin C-P, Wu I-L, Chen P-H, Tsay T-K. 2013. New TDR waveguides and data reduction method for monitoring of stream and drainage stage. *Journal of Hydrology* **505**: 346–351.

Church M, Hassan MA. 2002. Mobility of bed material in Harris Creek. *Water Resources Research* **38**(11): 1237. https://doi.org/10.1029/2001WR000753

Emmett WW, Leopold LB. 1963. Downstream pattern of riverbed scour and fill. *Proceedings of the Federal Interagency Sedimentation Conference*.

Geist DR, Dauble DD. 1998. Redd site selection and spawning habitat use by fall chinook salmon: the importance of geomorphic features in large rivers. *Environmental Management* **22**(5): 655–669.

Gendaszek AS, Magirl CS, Czuba CR, Konrad CP. 2013. The timing of scour and fill in a gravel-bedded river measured with buried accelerometers. *Journal of Hydrology* **495**: 186–196.

Gray JR, Laronne JB, Marr JDG. 2010. *Bedload-surrogate Monitoring Technologies*, US Geological Survey Scientific Investigations Report 2010–5091. US Geological Survey: Reston, VA; 37.

Haschenburger JK, Wilcock PR. 2003. Partial transport in a natural gravel bed channel. *Water Resources Research* **39**: 1020. https://doi.org/10.1029/2002WR001532

Hassan MA. 1990. Scour, fill, and burial depth of coarse material in gravel bed streams. *Earth Surface Processes and Landforms* **15**(4): 341–356.

Hausner MB, Suárez F, Glander KE, Giesen ND, Selker JS, Tyler SW. 2011. Calibrating single-ended fiber-optic Raman spectra distributed temperature sensing data. *Sensors* **11**(11): 10859–10879.

Hubbell DW. 1964. *Apparatus and Techniques for Measuring Bedload*, US Geological Survey Water-supply Paper 1748. US Geological Survey: Reston, VA; 74.

Kondolf GM, Wilcock PR. 1996. The flushing flow problem: defining and evaluating objectives. *Water Resources Research* **32**(8): 2589–2599.

Lamb MP, Dietrich WE, Venditti JG. 2008. Is the critical Shields stress for incipient sediment motion dependent on channel-bed slope? *Journal of Geophysical Research: Earth Surface* **113**, F02008. https://doi.org/10.1029/2007JF000831

Laronne J, Outhet D, Carling P, McCabe T. 1994. Scour chain employment in gravel bed rivers. *Catena* **22**(4): 299–306.

Leopold LB, Emmett WW. 1976. Bedload measurements, East Fork River, Wyoming. *Proceedings of the National Academy of Sciences* **73**(4): 1000–1004.

Luce CH, Tonina D, Gariglio F, Applebee R. 2013. Solutions for the diurnally forced advection-diffusion equation to estimate bulk fluid velocity and diffusivity in streambeds from temperature time series. *Water Resources Research* **49**(1): 488–506.

Meyer-Peter E, Müller R. 1948. *Formulas for Bed-load Transport*. International Association for Hydro-Environment Engineering and Research (IAHR): Stockholm.

Milan DJ, Heritage GL, Large AR, Fuller IC. 2011. Filtering spatial error from DEMs: implications for morphological change estimation. *Geomorphology* **125**(1): 160–171.

Miyata S, Fujita M. In Review. Laboratory experiment of continuous bedload monitoring in a retention basin of a steep mountain river: application of time domain reflectometry. *Earth Surface Processes and Landforms*.

Mueller ER, Pitlick J, Nelson JM. 2005. Variation in the reference Shields stress for bed load transport in gravel-bed streams and rivers. *Water Resources Research* **41**, W04006. https://doi.org/10.1029/2004WR003692

Rau GC, Cuthbert MO, McCallum AM, Halloran LJ, Andersen MS. 2015. Assessing the accuracy of 1-D analytical heat tracing for estimating near-surface sediment thermal diffusivity and water flux under transient conditions. *Journal of Geophysical Research: Earth Surface* **120**(8): 1551–1573.

Rickenmann D, McArdell BW. 2007. Continuous measurement of sediment transport in the Erlenbach stream using piezoelectric bedload impact sensors. *Earth Surface Processes and Landforms* **32**(9): 1362–1378.

Selker JS, Thevenaz L, Huwald H, Mallet A, Luxemburg W, Van De Giesen N, Stejskal M, Zeman J, Westhoff M, Parlange MB. 2006. Distributed fiber-optic temperature sensing for hydrologic systems. *Water Resources Research* **42**, W12202. https://doi.org/10.1029/2006WR005326

Singer MB, Dunne T. 2004. Modeling decadal bed material sediment flux based on stochastic hydrology. *Water Resources Research* **40**, W03302. https://doi.org/10.1029/2003WR002723

Stallman RW. 1965. Steady one-dimensional fluid flow in a semi-infinite porous medium with sinusoidal surface temperature. *Journal of Geophysical Research* **70**(12): 2821–2827.

Suárez F, Dozier J, Selker JS, Hausner MB, Tyler SW. 2011. *Heat Transfer in the Environment: Development and Use of Fiber-optic Distributed Temperature Sensing*. INTECH Open Access Publisher: Rijeka.

Tonina D, Luce C, Gariglio F. 2014. Quantifying streambed deposition and scour from stream and hyporheic water temperature time series. *Water Resources Research* **50**(1): 287–292.

Turowski JM, Badoux A, Rickenmann D. 2011. Start and end of bedload transport in gravel-bed streams. *Geophysical Research Letters* **38**, L04401. https://doi.org/10.1029/2010GL046558

Tyler SW, Selker JS, Hausner MB, Hatch CE, Torgersen T, Thodal CE, Schladow SG. 2009. Environmental temperature sensing using Raman spectra DTS fiber-optic methods. *Water Resources Research* **45**, W00D23. https://doi.org/10.1029/2008WR007052

US Bureau of Reclamation. 2008. *SRH-2D Theory and User's Manual version 2.0*, Prepared by Lai YG. Denver, CO.: Technical Service Center, Bureau of Reclamation.

US Bureau of Reclamation. 2013. *Flow Frequency Analysis of San Joaquin River below Friant Dam*, Water Resources and Operation Support Group, Technical Service Center, US Bureau of Reclamation Technical Memo, 6. Bureau of Reclamation: Denver, CO.

US Bureau of Reclamation. 2014a. *SJRRP Sediment Gradation Atlas, 1995–2012, Draft Version 2.1*. Bureau of Reclamation: Denver, CO.

US Bureau of Reclamation. 2014b. *Two-dimensional Modeling of Reach 1A of the San Joaquin River between Friant Dam and Highway 99*, Technical Report No. SRH-2014-14, Prepared by Gordon E, Greimann B, US Bureau of Reclamation, San Joaquin River Restoration Project Mid-Pacific Region. Bureau of Reclamation: Denver, CO; 48.

Wheaton JM, Brasington J, Darby SE, Sear DA. 2010. Accounting for uncertainty in DEMs from repeat topographic surveys: improved sediment budgets. *Earth Surface Processes and Landformd* **35**(2): 136–156.

Wilcock PR, Crowe JC. 2003. Surface-based transport model for mixed-size sediment. *Journal of Hydraulic Engineering* **129**(2): 120–128.

Wilcock PR, McArdell BW. 1997. Partial transport of a sand/gravel sediment. *Water Resources Research* **33**(1): 235–245.